

Subdiffraction incoherent optical imaging via spatial-mode demultiplexing: semiclassical treatment

Mankei Tsang*

Department of Electrical and Computer Engineering,

National University of Singapore, 4 Engineering Drive 3, Singapore 117583 and

Department of Physics, National University of Singapore, 2 Science Drive 3, Singapore 117551

(Dated: December 26, 2021)

I present a semiclassical analysis of a spatial-mode demultiplexing (SPADE) scheme for far-field incoherent optical imaging. Building on previous results that assume two point sources or the Gaussian point-spread function, I generalize SPADE for a larger class of point-spread functions and evaluate its errors in estimating the moments of an arbitrary subdiffraction object. Compared with the limits to direct imaging set by the Cramér-Rao bounds, the results show that SPADE can offer far superior accuracy in the subdiffraction regime for the second and higher-order moments.

I. INTRODUCTION

Recent theoretical and experimental studies have shown that far-field optical methods can substantially improve subdiffraction incoherent imaging [1–19]. While most of the prior works focus on two point sources, Ref. [8] proposes a spatial-mode demultiplexing (SPADE) measurement technique that can enhance the estimation of moments for arbitrary subdiffraction objects. Although the predicted enhancement is promising for applications in both astronomy and fluorescence microscopy, such as size and shape estimation for stellar or fluorophore clusters, researchers in those fields may find it difficult to comprehend the quantum formalism used in Ref. [8]. One of the main goals of this work is therefore to introduce a more accessible semiclassical formalism that can reproduce the results there, assuming only a background knowledge of statistical optics on the level of Goodman [20, 21] and parameter estimation on the level of Van Trees [22]. The formalism incorporates diffraction, photon shot noise, and—most importantly—coherent optical processing, which enables the enhancements proposed in Refs. [1–19]. This work thus sheds light on the physical origin of the enhancements, clarifying that no exotic quantum phenomenon is needed to explain or implement them.

As Ref. [8] assumes the Gaussian PSF exclusively, another goal of this work is to generalize the results for a larger class of point-spread functions (PSFs) via the theory of orthogonal polynomials [15, 23], affirming that enhancement remains possible in those cases. To set a benchmark for the proposed method, I derive limits to direct imaging in the subdiffraction and shot-noise-limited regime in the form of Cramér-Rao bounds (CRBs) [22, 24–29], which may be of independent interest to image-processing and deconvolution research [30–40]. On a more technical level, this work also investigates the estimation bias introduced by an approximation made in Ref. [8] and assures that it is harmless.

This paper is organized as follows. Section II introduces the background formalism of statistical optics, measurement noise, and CRBs. Section III derives the CRBs for moment estimation via direct imaging of a subdiffraction object. Section IV presents a design of SPADE for a general class of PSFs and evaluates the biases and errors of the proposed method for moment estimation, showing that giant accuracy enhancements are possible for the second and higher-order moments. Section V revisits the case of Gaussian PSF studied in Ref. [8] and also proposes new exactly unbiased estimators in the case of two dimensions. Section VI presents a Monte Carlo analysis to confirm the theory. Section VII concludes the paper, pointing out open questions and future directions. Appendix A introduces the multi-index notation that is used throughout this paper, while Appendix B proves the mathematical properties of some matrices in the main text.

II. FORMALISM

A. Statistical optics

Consider the paraxial theory of quasi-monochromatic scalar waves and a spatially incoherent object distribution [20, 21]. On the image plane of a diffraction-limited imaging system—depicted in Fig. 1—the mutual coherence function, also called the mutual intensity, can be expressed as [20, 21]

$$\Gamma(x, x' | \theta) = \int dX \psi(x - X) \psi^*(x' - X) F(X | \theta), \quad (2.1)$$

where $x, x' \in \mathbb{R}^D$ are D -dimensional position vectors on the image plane, X is the object-plane position vector normalized with respect to the magnification factor, $F(X | \theta)$ is the object intensity distribution, $\theta = (\theta_0, \theta_1, \dots)$ is a vector of unknown parameters to be estimated, and $\psi(x)$ is the PSF for the field. To simplify the notations, I adopt the multi-index notation described in Appendix A and Ref. [23], such that D can be kept arbitrary, though $D = 1$ or 2 is typical in spectroscopy

* mankei@nus.edu.sg

and imaging. Note that three-dimensional imaging requires a different formalism and is outside the scope of this paper; D is kept arbitrary simply in case the mathematical results here have applications besides imaging. The average intensity distribution on the image plane is

$$f(x|\theta) \equiv \Gamma(x, x|\theta) = \int dX |\psi(x - X)|^2 F(X|\theta), \quad (2.2)$$

which is a basic result in statistical optics [20, 21].

For convenience, I normalize the position vectors with respect to the width of the PSF, such that the PSF width is equal to 1 in this unit. The PSF is assumed to obey the normalization

$$\int dx |\psi(x)|^2 = 1, \quad (2.3)$$

such that

$$\theta_0 \equiv \int dX F(X|\theta) = \int dx f(x|\theta) \quad (2.4)$$

is the total optical power reaching the image plane on average. Unlike the normalization $\theta_0 = 1$ in Ref. [8], I assume here that θ_0 is an unknown parameter for generality.

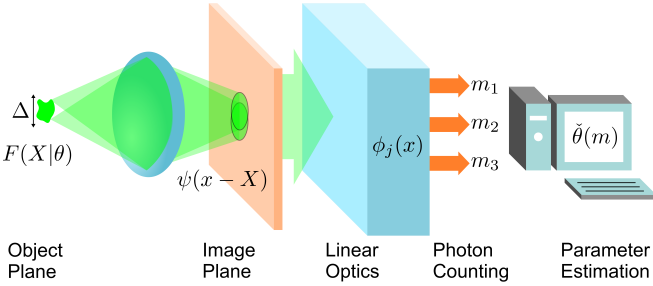


FIG. 1. (Color online). A far-field optical imaging system with additional optical processing after the image plane. See the main text for the definitions of the expressions.

Instead of intensity measurement on the image plane, consider the use of further linear optics to process the field followed by photon counting in each output channel, as depicted in Fig. 1. The average power in each output channel can be expressed as

$$p_j(\theta) = \int dx \int dx' \phi_j^*(x) \phi_j(x') \Gamma(x, x'|\theta) \quad (2.5)$$

$$= \int dX |h_j(X)|^2 F(X|\theta), \quad (2.6)$$

where $\phi_j^*(x)$ is a propagator that couples the image-plane field from position x to the j th output, and

$$h_j(X) \equiv \int dx \phi_j^*(x) \psi(x - X) \quad (2.7)$$

is another propagator that couples the object-plane field at X to the j th output. If the optics after the image

plane is passive but lossless, power conservation implies that

$$\sum_j p_j(\theta) = \theta_0, \quad (2.8)$$

and $\phi_j(x)$ must be unitary, or

$$\sum_j \phi_j(x) \phi_j^*(x') = \delta(x - x'), \quad (2.9)$$

$$\int dx \phi_j(x) \phi_k^*(x) = \delta_{jk}. \quad (2.10)$$

In other words, $\{\phi_j(x)\}$ is an orthonormal basis, and each output can be regarded as a projection of the image-plane field in a spatial mode [3, 41]. For example, direct imaging, which measures the spatial intensity distribution on the image plane, can be modeled by taking $\phi_j(x) = \sqrt{dx} \delta(x_j - x)$, where x_j is the position of each pixel with infinitesimal area dx , such that $p_j(\theta) = f(x_j|\theta)dx$. A generalization of the measurement model using the concept of positive operator-valued measures is possible even within the semiclassical formalism [3] but not needed here.

In superresolution research, it is well known that object reconstruction via a singular-value decomposition (SVD) technique can achieve arbitrary superresolution if $f(x|\theta)$ is measured exactly and the object size is limited [30, 31]. The caveat is that the technique performs poorly in the presence of noise, so it is imperative to employ proper statistics to study the problem. For weak incoherent sources, such as astronomical optical sources and microscopic fluorophores, bunching or antibunching is negligible, and it is standard to assume a Poisson model for the photon counts $m = (m_1, m_2, \dots)$ at the output channels [3, 21, 25, 26, 28, 32, 42]. The Poisson distribution is

$$P(m|\theta) = \prod_j \exp[-\tau p_j(\theta)] \frac{[\tau p_j(\theta)]^{m_j}}{m_j!}, \quad (2.11)$$

where τ is a conversion factor given by

$$\tau = \frac{\eta T}{\hbar \omega_0}, \quad (2.12)$$

$\eta \in [0, 1]$ is the quantum efficiency, T is the allowed integration time, and $\hbar \omega_0$ is the photon energy. The most important statistics here are the mean

$$\mathbb{E}(m) = \tau p(\theta), \quad (2.13)$$

where \mathbb{E} denotes the expectation with respect to P , and the covariance matrix

$$\mathbb{V}_{jk}(m) \equiv \mathbb{E}[m_j - \mathbb{E}(m_j)][m_k - \mathbb{E}(m_k)] \quad (2.14)$$

$$= \mathbb{E}(m_j) \delta_{jk}, \quad (2.15)$$

which is signal-dependent. The total photon number detected by the measurement on average is

$$N \equiv \sum_j \mathbb{E}(m_j) = \tau \theta_0 \leq N_0 \equiv \frac{T \theta_0}{\hbar \omega_0}, \quad (2.16)$$

where N_0 is the total number arriving at the image plane on average. Conditioned on a total photon number, m obeys a multinomial distribution, and the reconstruction of F via direct imaging becomes the density deconvolution problem in nonparametric statistics; see, for example, Refs. [38–40] and references therein.

The quantum formalism arrives at the same Poisson model by assuming that the average photon number per spatiotemporal mode is much smaller than 1 and the photon count for each channel is integrated over multiple temporal modes [1, 8]. That said, an advantage of the semiclassical model besides simplicity is that it applies to any source that produces Poisson noise at the output, such as incoherent laser sources [21] and electron microscopy [42], without the need to check all the assumptions for the quantum model.

B. Cramér-Rao bounds (CRBs)

Owing to the signal-dependent nature of Poisson noise, the linear SVD approach to superresolution [30, 31] is inadequate here. A more suitable tool is the CRB, which is now standard in modern astronomy [25–27] and fluorescence microscopy [28, 29]. For any estimator $\check{\theta}(m)$ that satisfies the unbiased condition

$$\mathbb{E}(\check{\theta}) = \theta, \quad (2.17)$$

the mean-square error matrix is equal to its covariance, viz.,

$$\text{MSE}_{\mu\nu}(\check{\theta}, \theta) \equiv \mathbb{E}(\check{\theta}_\mu - \theta_\mu)(\check{\theta}_\nu - \theta_\nu) = \mathbb{V}_{\mu\nu}(\check{\theta}), \quad (2.18)$$

and the CRB is given by [22, 24–29]

$$\text{MSE}_{\mu\mu}(\check{\theta}, \theta) \geq \text{CRB}_{\mu\mu}(\theta), \quad (2.19)$$

where

$$\text{CRB}(\theta) \equiv J^{-1}(\theta) \quad (2.20)$$

is the inverse of the Fisher information matrix defined as

$$J_{\mu\nu}(\theta) \equiv \sum_m \frac{1}{P(m|\theta)} \frac{\partial P(m|\theta)}{\partial \theta_\mu} \frac{\partial P(m|\theta)}{\partial \theta_\nu}. \quad (2.21)$$

In the limit of infinite trials, the maximum-likelihood estimator is asymptotically unbiased with a covariance equal to the CRB [22, 24].

For the Poisson model, the Fisher information is given by

$$J_{\mu\nu}(\theta) = \tau \sum_j \frac{1}{p_j(\theta)} \frac{\partial p_j(\theta)}{\partial \theta_\mu} \frac{\partial p_j(\theta)}{\partial \theta_\nu}. \quad (2.22)$$

For example, the information for ideal direct imaging with infinitesimal pixel size is

$$J_{\mu\nu}(\theta) = \tau \int dx \frac{1}{f(x|\theta)} \frac{\partial f(x|\theta)}{\partial \theta_\mu} \frac{\partial f(x|\theta)}{\partial \theta_\nu}. \quad (2.23)$$

An intuitive way of understanding Eq. (2.22) is to regard it as a signal-to-noise ratio: each derivative $\partial p_j(\theta)/\partial \theta_\mu$ measures the sensitivity of a channel to a parameter, and the denominator $p_j(\theta)$, proportional to the Poisson variance, indicates the noise level. The form of Eq. (2.22) hence suggests that any parameter-insensitive background in $p_j(\theta)$ should be minimized.

The Bayesian CRB (BCRB) can be used to set more general limits for any biased or unbiased estimator [6, 22, 43–45]. Define the Bayesian mean-square error as

$$\text{BMSE}(\check{\theta}) \equiv \int d\theta \Pi(\theta) \text{MSE}(\check{\theta}, \theta), \quad (2.24)$$

where $\Pi(\theta)$ is a prior probability density. For any prior that vanishes on the boundary of its domain, the BCRB is given by

$$\text{BMSE}_{\mu\mu}(\check{\theta}) \geq \text{BCRB}_{\mu\mu}, \quad (2.25)$$

$$\text{BCRB} \equiv (\tilde{J} + j)^{-1}, \quad (2.26)$$

where

$$\tilde{J} \equiv \int d\theta \Pi(\theta) J(\theta) \quad (2.27)$$

is the Fisher information averaged over the prior and

$$j_{\mu\nu} \equiv \int d\theta \frac{1}{\Pi(\theta)} \frac{\partial \Pi(\theta)}{\partial \theta_\mu} \frac{\partial \Pi(\theta)}{\partial \theta_\nu} \quad (2.28)$$

is the prior information. Other Bayesian bounds for more general priors can be found in Ref. [45]. The BCRB also applies to the worst-case error $\sup_\theta \text{MSE}_{\mu\mu}(\check{\theta}, \theta)$ for minimax estimation [6, 44], since

$$\sup_\theta \text{MSE}_{\mu\mu}(\check{\theta}, \theta) \geq \text{BMSE}_{\mu\mu}(\check{\theta}) \quad (2.29)$$

for any $\Pi(\theta)$, and the prior can be chosen to tighten the bound [6, 44].

The BCRB is close to the CRB if $J(\theta)$ is parameter-independent, such that $\tilde{J} = J$, and the prior information j is negligible relative to \tilde{J} , such that

$$\text{BCRB} = (\tilde{J} + j)^{-1} \approx \tilde{J}^{-1} = J^{-1}. \quad (2.30)$$

A counterexample is the problem of two-point resolution [6], where $J(\theta)$ for separation estimation via direct imaging vanishes at a point in the parameter space, making the BCRB very sensitive to the choice of prior. This issue depends on the parameterization [44] and does not arise here, however, as the next section shows.

III. LIMITS TO DIRECT IMAGING

A. Parameterization

Following Ref. [8], I consider the object moments

$$\theta_\mu \equiv \int dX X^\mu F(X|\theta), \quad \mu \in \mathbb{N}_0^D \quad (3.1)$$

as the parameters. Unlike the $\theta_0 = 1$ assumption in Ref. [8], however, $F(X|\theta)$ and therefore the moments are unnormalized here. Generalizing the use of Hermite polynomials for the Gaussian PSF in Ref. [8], I consider orthogonal polynomials with respect to the centered PSF $|\psi(x)|^2$ as the weight function [23]. I write the set of polynomials as

$$a \equiv \{a_\mu(x); \mu \in \mathbb{N}_0^D\}, \quad (3.2)$$

where

$$a_\mu(x) = \sum_\nu A_{\mu\nu} x^\nu \quad (3.3)$$

is a polynomial of degree $|\mu|$ and the multi-index notation in Appendix A is adopted. A is an invertible matrix that satisfies the lower-triangular property

$$A_{\mu\nu} = 0 \text{ if } \nu > \mu, \quad (3.4)$$

assuming the graded lexicographical order [23]

$$\begin{aligned} \nu > \mu &\Leftrightarrow |\nu| > |\mu|, \text{ or if } |\nu| = |\mu|, \\ &\text{the first nonzero } \nu_j - \mu_j > 0. \end{aligned} \quad (3.5)$$

The polynomials are defined by the orthonormal condition

$$\int dx |\psi(x)|^2 a_\mu(x) a_\nu(x) = \delta_{\mu\nu}. \quad (3.6)$$

Appendix B describes a way of computing A via Cholesky decomposition.

Using the orthonormality of a , I can expand the shifted PSF as

$$|\psi(x - X)|^2 = |\psi(x)|^2 \sum_\mu a_\mu(x) b_\mu(X), \quad (3.7)$$

where

$$b_\mu(X) \equiv \int dx a_\mu(x) |\psi(x - X)|^2. \quad (3.8)$$

With a change of variable $u = x - X$, it is easy to show that $b_\mu(X)$ is also a polynomial, viz.,

$$b_\mu(X) = \sum_\nu B_{\mu\nu} X^\nu, \quad (3.9)$$

where B is another invertible and lower-triangular matrix given by

$$B_{\mu\nu} = \partial_X^\nu b_\mu(X)|_{X=0} = \frac{1}{\nu!} \int dx |\psi(x)|^2 \partial^\nu a_\mu(x), \quad (3.10)$$

as shown in Appendix B. The average image given by Eq. (2.2) becomes

$$f(x|\theta) = |\psi(x)|^2 \sum_\mu a_\mu(x) \beta_\mu(\theta), \quad (3.11)$$

where I have defined

$$\beta_\mu(\theta) \equiv \int dX b_\mu(X) F(X|\theta) \quad (3.12)$$

as another set of parameters. In terms of the moments, β_μ can be rewritten as

$$\beta_\mu = \sum_\nu B_{\mu\nu} \theta_\nu, \quad (3.13)$$

using Eq. (3.9). Under general conditions [23], the set of moments uniquely determine the distribution F , so the invertibility of B implies that the β parameters also determine F uniquely. The pointwise reconstruction of a subdiffraction F with noise is a notorious problem [30, 31, 34, 35, 38–40] and outside the scope of this paper, however, and I focus on moment estimation hereafter.

B. Cramér-Rao bounds

Define $\{dm(x); x \in \mathbb{R}^D\}$ as the measurement record from direct imaging with infinitesimal pixel size, Poisson statistics, and an expected value given by

$$\mathbb{E}[dm(x)] = \tau f(x|\theta) dx. \quad (3.14)$$

The Fisher information matrix with respect to β_μ is

$$J_{\mu\nu}^{(\beta)} = \tau \int dx \frac{1}{f(x|\theta)} \frac{\partial f(x|\theta)}{\partial \beta_\mu} \frac{\partial f(x|\theta)}{\partial \beta_\nu}. \quad (3.15)$$

The data-processing inequality [46] ensures that increasing the pixel size, or any processing of the image-plane intensity in general, can only lower the amount of information. Define the object width as the minimum Δ such that

$$F(X|\theta) = 0 \text{ if } \|X\| > \frac{\Delta}{2}, \quad (3.16)$$

and define the subdiffraction regime as the scenario where Δ is much smaller than the width of the PSF, or

$$\Delta \ll 1 \quad (3.17)$$

in the dimensionless unit assumed here. This can be regarded as the opposite to the sparse regime commonly assumed in compressed sensing [33–36]. It simplifies the calculation here and can be ensured by prior information in practice, but note that it can be relaxed if a more specific parametric model is adopted, such as the two-point model.

The moments observe a magnitude hierarchy as

$$|X^\mu| \leq \left(\frac{\Delta}{2}\right)^{|\mu|}, \quad (3.18)$$

$$|\theta_\mu| \leq \int dX |X^\mu| F(X|\theta) \leq \theta_0 \left(\frac{\Delta}{2}\right)^{|\mu|}, \quad (3.19)$$

and the average image can be expressed as

$$f(x|\theta) = \sum_{\mu} \frac{\theta_{\mu}}{\mu!} (-\partial)^{\mu} |\psi(x)|^2 \quad (3.20)$$

$$= \theta_0 |\psi(x)|^2 [1 + O(\Delta)], \quad (3.21)$$

meaning that the image resembles the centered PSF to the zeroth order. Substituting Eq. (3.11) into the derivatives of Eq. (3.15) and Eq. (3.21) into the denominator of Eq. (3.15), I obtain

$$J_{\mu\nu}^{(\beta)} = \frac{\tau}{\theta_0} \int dx \frac{|\psi(x)|^2 a_{\mu}(x) a_{\nu}(x)}{1 + O(\Delta)} \quad (3.22)$$

$$= \frac{\tau}{\theta_0} [\delta_{\mu\nu} + O(\Delta)], \quad (3.23)$$

where the orthonormality of a given by Eq. (3.6) is used. The CRB becomes

$$\text{CRB}_{\mu\nu}^{(\beta)} = \frac{\theta_0}{\tau} [\delta_{\mu\nu} + O(\Delta)]. \quad (3.24)$$

To approach the CRB, consider the linear and unbiased estimator

$$\check{\beta}_{\mu} = \frac{1}{\tau} \int dm(x) a_{\mu}(x). \quad (3.25)$$

Its covariance is

$$\mathbb{V}_{\mu\nu}(\check{\beta}) = \frac{1}{\tau} \int dx f(x|\theta) a_{\mu}(x) a_{\nu}(x) \quad (3.26)$$

$$= \frac{\theta_0}{\tau} \int dx |\psi(x)|^2 [1 + O(\Delta)] a_{\mu}(x) a_{\nu}(x) \quad (3.27)$$

$$= \frac{\theta_0}{\tau} [\delta_{\mu\nu} + O(\Delta)], \quad (3.28)$$

which is equal to the CRB in the leading order.

For moment estimation, the Fisher information can be obtained via the parameter transformation given by Eq. (3.13), viz.,

$$J_{\mu\nu} = \sum_{\xi, \zeta} \frac{\partial \beta_{\xi}}{\partial \theta_{\mu}} J_{\xi\zeta}^{(\beta)} \frac{\partial \beta_{\zeta}}{\partial \theta_{\nu}} \quad (3.29)$$

$$= \sum_{\xi, \zeta} B_{\xi\mu} J_{\xi\zeta}^{(\beta)} B_{\zeta\nu} \quad (3.30)$$

$$= \frac{\tau}{\theta_0} \left[\sum_{\xi} B_{\xi\mu} B_{\xi\nu} + O(\Delta) \right]. \quad (3.31)$$

Since B is invertible, the CRB becomes

$$\text{CRB}_{\mu\nu} = \frac{\theta_0}{\tau} \left[\sum_{\xi} (B^{-1})_{\mu\xi} (B^{-1})_{\nu\xi} + O(\Delta) \right]. \quad (3.32)$$

A linear, unbiased, and near-efficient estimator can be constructed as

$$\check{\theta}_{\mu} = \sum_{\nu} (B^{-1})_{\mu\nu} \check{\beta}_{\nu}, \quad (3.33)$$

and its variance is

$$\mathbb{V}_{\mu\nu}(\check{\theta}) = \frac{\theta_0}{\tau} \left[\sum_{\xi} (B^{-1})_{\mu\xi} (B^{-1})_{\nu\xi} + O(\Delta) \right], \quad (3.34)$$

which is equal to the CRB in the leading order.

To generalize the CRB for any biased or unbiased estimator, consider the BCRB described in Sec. II B. As the Fisher information given by Eq. (3.31) depends only on θ_0 and not the other parameters to the leading order, the average information \tilde{J} defined by Eq. (2.27) is relatively insensitive to the choice of prior in the subdiffraction regime. For any reasonable prior that gives a finite prior information j , a long enough integration time can then make \tilde{J} much larger than j in Eq. (2.26), leading to $\text{BCRB} \approx \text{CRB}$, with θ_0 replaced by $1/\int d\theta_0 \Pi(\theta_0)(1/\theta_0)$. The CRB and the BCRB hence give similar results here in the asymptotic limit, unlike the issue encountered in Ref. [6].

The CRBs in this section set fundamental limits to image-processing algorithms [30–37, 40] in the subdiffraction and shot-noise-limited regime. The next section shows that coherent optical processing can beat them.

IV. SPATIAL-MODE DEMULTIPLEXING (SPADE)

A. Point-spread-function-adapted (PAD) basis

References [1–19] have shown that SPADE, a technique of linear optics and photon counting with respect to a judiciously chosen basis of spatial modes, can substantially improve subdiffraction imaging. To generalize the use of the transverse-electromagnetic (TEM) basis in Ref. [8], I consider the point-spread-function-adapted (PAD) basis proposed by Rehacek *et al.* for the two-point problem [15] and apply it to more general objects. Denote the basis by

$$\{\phi_q(x); q \in \mathbb{N}_0^D\}, \quad (4.1)$$

where the spatial modes are more conveniently defined in the spatial-frequency domain. Defining

$$\Phi_q(k) \equiv \frac{1}{(2\pi)^{d/2}} \int dk \phi_q(x) \exp(-ik \cdot x), \quad (4.2)$$

$$\Psi(k) \equiv \frac{1}{(2\pi)^{d/2}} \int dk \psi(x) \exp(-ik \cdot x), \quad (4.3)$$

$\Phi_q(k)$ can be expressed as

$$\Phi_q(k) = (-i)^{|q|} c_q(k) \Psi(k), \quad (4.4)$$

$$c_q(k) \equiv \sum_r C_{qr} k^r, \quad (4.5)$$

where $\{c_q(k); q \in \mathbb{N}_0^D\}$ is a set of real orthogonal polynomials with $|\Psi(k)|^2$ as the weight function [23] and C is

an invertible lower-triangular matrix. The orthonormal condition used to define the polynomials is

$$\int dk \Phi_q^*(k) \Phi_r(k) = \int dk |\Psi(k)|^2 c_q(k) c_r(k) = \delta_{qr}. \quad (4.6)$$

Equation (4.6) also ensures that $\{\phi_q(x)\}$ is an orthonormal basis. As $\phi_0(x) = \psi(x)$ and each higher-order mode in real space is a sum of $\psi(x)$ derivatives given by

$$\phi_q(x) = (-i)^{|q|} c_q(-i\partial) \psi(x), \quad (4.7)$$

the PAD basis can be regarded as a generalization of the binary SPADE concept in Ref. [1] and the derivative-mode concept in Ref. [14]. Appendix B contains more mathematical properties of C .

In terms of the PAD basis, I can define the mutual coherence matrix

$$\Gamma_{qq'}(\theta) \equiv \int dX h_q(X) h_{q'}^*(X) F(X|\theta), \quad (4.8)$$

where the propagator $h_q(X)$ is defined by Eq. (2.7). In particular, SPADE in the PAD basis gives a set of photon counts $\{m_q; q \in \mathbb{N}_0^D\}$ with expected value

$$\mathbb{E}(m_q) = \tau_0 \Gamma_{qq}, \quad (4.9)$$

where τ_0 denotes the conversion factor for the PAD-basis measurement. An unbiased estimator of Γ_{qq} is

$$\check{\Gamma}_{qq} = \frac{m_q}{\tau_0}, \quad (4.10)$$

with variance

$$\mathbb{V}(\check{\Gamma}_{qq}) = \frac{\Gamma_{qq}}{\tau_0}. \quad (4.11)$$

To access the off-diagonal components of Γ , take two spatial modes with indices q and q' from the PAD basis and interfere them, such that the outputs correspond to projections into the spatial modes

$$\varphi_{qq'}^+(x) = \frac{1}{\sqrt{2}} [\phi_q(x) + \phi_{q'}(x)], \quad (4.12)$$

$$\varphi_{qq'}^-(x) = \frac{1}{\sqrt{2}} [\phi_q(x) - \phi_{q'}(x)], \quad (4.13)$$

which I call the interferometric-PAD (iPAD) modes. The photon counts at the two outputs, denoted by $m_{qq'}^+$ and $m_{qq'}^-$, have the expected values

$$\mathbb{E}(m_{qq'}^+) = \tau_j \left(\frac{\Gamma_{qq} + \Gamma_{q'q'}}{2} + \text{Re} \Gamma_{qq'} \right), \quad (4.14)$$

$$\mathbb{E}(m_{qq'}^-) = \tau_j \left(\frac{\Gamma_{qq} + \Gamma_{q'q'}}{2} - \text{Re} \Gamma_{qq'} \right), \quad (4.15)$$

where τ_j denotes another conversion factor, since projections in the iPAD modes, being linearly dependent on the original PAD modes, must be performed separately from

the PAD-basis measurement, either sequentially in time or on beamsplitted light. Assume further that $|\Psi(k)|^2$ is centrally symmetric, as defined by

$$|\Psi(k)|^2 = |\Psi(-k)|^2, \quad (4.16)$$

such that C , $h_q(X)$, and $\Gamma_{qq'}$ are all real, as shown in Appendix B and assumed hereafter. An unbiased estimator of $\Gamma_{qq'}$ is then

$$\check{\Gamma}_{qq'} = \frac{m_{qq'}^+ - m_{qq'}^-}{2\tau_j}, \quad (4.17)$$

with

$$\mathbb{V}(\check{\Gamma}_{qq'}) = \frac{\Gamma_{qq} + \Gamma_{q'q'}}{4\tau_j}. \quad (4.18)$$

While it is not yet obvious that $\Gamma_{qq'}$ is a useful set of parameters for imaging, the next sections will show that they can be used to estimate the object moments with superior accuracy.

B. Moment estimation

To relate the PAD-basis mutual coherence matrix $\Gamma_{qq'}$ to the object moments, use Eqs. (2.7) and (4.2)–(4.4) to rewrite the propagator $h_q(X)$ as

$$h_q(X) = i^{|q|} \int dk |\Psi(k)|^2 c_q(k) \exp(-ik \cdot X) \quad (4.19)$$

$$= i^{|q|} \int dk |\Psi(k)|^2 c_q(k) \sum_r \frac{(-ik)^r X^r}{r!} \quad (4.20)$$

$$= \sum_r H_{qr} X^r, \quad (4.21)$$

where

$$H_{qr} \equiv \frac{i^{|q|}}{r!} \int dk |\Psi(k)|^2 c_q(k) (-ik)^r \quad (4.22)$$

$$= \frac{i^{|q|} (-i)^{|r|}}{r!} (C^{-1})_{rq}, \quad (4.23)$$

$$(H^{-1})_{qr} = q! i^{|q|} (-i)^{|r|} C_{rq}, \quad (4.24)$$

as shown in Appendix B. Since C^{-1} and C are lower-triangular, H and H^{-1} are upper-triangular, viz.,

$$H_{qr} = 0, (H^{-1})_{qr} = 0 \text{ if } r < q, \quad (4.25)$$

and $h_q(X)$ consists of monomials $\{X^r; r \geq q\}$ with degrees at least as high as $|q|$. The magnitudes of $h_q(X)$ and $\Gamma_{qq'}$ can then be expressed as

$$h_q(X) = O(\Delta^{|q|}), \quad (4.26)$$

$$\Gamma_{qq'} = \theta_0 O(\Delta^{|q+q'|}), \quad (4.27)$$

and the variances given by Eqs. (4.11) and (4.18) become

$$\mathbb{V}(\tilde{\Gamma}_{qq'}) = \frac{\theta_0}{\tau_j} O(\Delta^{2\min(|q|, |q'|)}). \quad (4.28)$$

Substituting Eq. (4.21) into Eq. (4.8), $\Gamma_{qq'}$ can be related to the moments by

$$\Gamma_{qq'} = \sum_{r, r'} H_{qr} H_{q'r'} \theta_{r+r'}, \quad (4.29)$$

which can be inverted to give

$$\theta_{q+q'} = \sum_{r, r'} \Upsilon_{qq'rr'} \Gamma_{rr'}, \quad (4.30)$$

$$\Upsilon_{qq'rr'} \equiv (H^{-1})_{qr} (H^{-1})_{q'r'}. \quad (4.31)$$

This linear relation implies that an unbiased estimator of $\theta_{q+q'}$ can be constructed from unbiased estimators of $\Gamma_{pp'}$ given by Eqs. (4.10) and (4.17), viz.,

$$\check{\theta}_{q+q'} = \sum_{r, r'} \Upsilon_{qq'rr'} \check{\Gamma}_{rr'}. \quad (4.32)$$

Since $\Upsilon_{qq'rr'}$ is nonzero only for $r \geq q$ and $r' \geq q'$, I can write the variance of Eq. (4.32) as

$$\mathbb{V}(\check{\theta}_{q+q'}) = \sum_{r, r'} \Upsilon_{qq'rr'}^2 \mathbb{V}(\check{\Gamma}_{rr'}) \quad (4.33)$$

$$= \frac{\theta_0}{\min(\tau_j)} O(\Delta^{2\min(|q|, |q'|)}), \quad (4.34)$$

using Eq. (4.28). While the dependence on $O(\Delta^{2\min(|q|, |q'|)})$ suggests that a judicious choice of $|q|$ and $|q'|$ can make the variance substantially lower than the direct-imaging CRB given by Eq. (3.32), the dependence on $\min(\tau_j)$ is a problem. In general, measurements in incompatible bases must be performed sequentially or separately on beamsplitted light. If each measurement has a conversion factor τ_j , energy conservation requires

$$\sum_j \tau_j \leq \frac{T}{\hbar\omega_0}, \quad (4.35)$$

so $\min(\tau_j)$ in Eq. (4.34) may be too small if the spatial modes needed to implement Eq. (4.33) cannot be grouped into a reasonable number of bases. An exception—seemingly fortuitous—occurs in the case of two-dimensional Gaussian PSF, for which 7 bases are sufficient to construct unbiased estimators of all moments, as elaborated later in Sec. VC.

To find a simpler estimator in the general case, first use the property $H_{qr} = 0$ for $r < q$ to rewrite Eq. (4.30) as

$$\begin{aligned} \theta_{q+q'} &= \sum_{|r|=|q|, |r'|=|q'|} \Upsilon_{qq'rr'} \Gamma_{rr'} \\ &+ \sum_{|r+r'| > |q+q'|} \Upsilon_{qq'rr'} \Gamma_{rr'}, \end{aligned} \quad (4.36)$$

which expresses $\theta_{q+q'}$ as a sum of $\theta_0 O(\Delta^{|q+q'|})$ terms and higher-order terms, as ranked by Eq. (4.27). To evaluate the magnitude of the higher-order terms, note that, for a centrally symmetric $|\Psi(k)|^2$, $(H^{-1})_{qr} \propto C_{rq} = 0$ if $|r| = |q| + 1, |q| + 3, \dots$ [23], so

$$\sum_{|r+r'| > |q+q'|} \Upsilon_{qq'rr'} \Gamma_{rr'} = \theta_0 O(\Delta^{|q+q'|+2}). \quad (4.37)$$

A simplified estimator can then be constructed as

$$\check{\theta}'_{q+q'} = \sum_{|r|=|q|, |r'|=|q'|} \Upsilon_{qq'rr'} \check{\Gamma}_{rr'}, \quad (4.38)$$

which ensures that only a finite number of $\check{\Gamma}_{rr'}$'s and a finite number of measurement bases are needed. The bias is the negative of Eq. (4.37), viz.,

$$\mathbb{E}(\check{\theta}'_{q+q'}) - \theta_{q+q'} = \theta_0 O(\Delta^{|q+q'|+2}), \quad (4.39)$$

the magnitude of which is much smaller than that of the parameter $|\theta_{q+q'}| = \theta_0 O(\Delta^{|q+q'|})$, while the variance is

$$\mathbb{V}(\check{\theta}'_{q+q'}) = \sum_{|r|=|q|, |r'|=|q'|} \Upsilon_{qq'rr'}^2 \mathbb{V}(\check{\Gamma}_{rr'}) \quad (4.40)$$

$$= \frac{\theta_0}{\min(\tau_j)} O(\Delta^{2\min(|q|, |q'|)}), \quad (4.41)$$

which is lower than Eq. (4.33) but on the same order of magnitude. To minimize this variance for a given moment θ_μ , $\min(|q|, |q'|)$ should be made as high as possible. This can be accomplished by choosing

for each $j \in \{1, 2, \dots, D\}$,

$$q_j = \begin{cases} \mu_j/2 & \text{if } \mu_j \text{ is even,} \\ \lfloor \mu_j/2 \rfloor & \text{if } \mu_j \text{ is the first odd number,} \\ \lceil \mu_j/2 \rceil & \text{if } \mu_j \text{ is odd and the last choice was } \lfloor \cdot \rfloor, \\ \lfloor \mu_j/2 \rfloor & \text{if } \mu_j \text{ is odd and the last choice was } \lceil \cdot \rceil. \end{cases} \quad (4.42)$$

The alternating floor and ceil operations keep $|q|$ high without exceeding $|q'|$. If $|\mu|$ is even, μ has an even number of odd entries, then $|q| = |q'| = |\mu|/2$. If $|\mu|$ is odd, μ has an odd number of odd entries, then $|q| = (|\mu| - 1)/2$ and $|q'| = (|\mu| + 1)/2$. Hence one can achieve

$$\min(|q|, |q'|) = \left\lfloor \frac{|\mu|}{2} \right\rfloor, \quad (4.43)$$

$$\mathbb{V}(\check{\theta}'_\mu) = \frac{\theta_0}{\min(\tau_j)} O(\Delta^{2\lfloor |\mu|/2 \rfloor}). \quad (4.44)$$

The mean-square error is hence

$$\text{MSE}(\check{\theta}'_\mu, \theta_\mu) = \mathbb{V}(\check{\theta}'_\mu) + [\mathbb{E}(\check{\theta}'_\mu) - \theta_\mu]^2 \quad (4.45)$$

$$= \frac{\theta_0}{\min(\tau_j)} O(\Delta^{2\lfloor |\mu|/2 \rfloor}) + \theta_0^2 O(\Delta^{2|\mu|+4}). \quad (4.46)$$

Compared with the CRB for direct imaging given by Eq. (3.32), Eq. (4.46) can be much lower in the $\Delta \ll 1$ subdiffraction regime if $|\mu| \geq 2$, $\min(\tau_j)$ is on the same order of magnitude as the τ for direct imaging, and the bias is negligible.

A heuristic explanation of the enhancement is as follows. Recall that Poisson noise is signal-dependent, and any background in the signal increases the variance and reduces the signal-to-noise ratio. In the subdiffraction regime, the direct image is so blurred that it resembles the centered PSF $|\psi(x)|^2$, and the fundamental mode $\phi_0(x) = \psi(x)$ acts as a background and the main contributor of noise. On the other hand, each PAD or iPAD spatial mode is sensitive to moments above a certain order only, so it is immune from the background noises caused by the lower-order modes.

C. Criterion for informative estimation

A word of caution is in order: even with SPADE, there are severe resolution limits. This is because the moments are inherently small parameters in the subdiffraction regime according to Eq. (3.19), and the error needs to be much smaller than the prior range of the parameter for the estimation to be informative. To be specific, I adopt the Bayesian perspective [22, 45, 47] and consider the Bayesian error given by Eq. (2.24). In the absence of measurements, the error is determined by the prior and given by

$$\text{BMSE}_{\mu\mu}^{(\Pi)} \equiv \mathbb{E}^{(\Pi)} \left[\theta_\mu - \mathbb{E}^{(\Pi)}(\theta_\mu) \right]^2 \leq \theta_0^2 \left(\frac{\Delta}{2} \right)^{2|\mu|}, \quad (4.47)$$

where $\mathbb{E}^{(\Pi)}$ denotes expectation with respect to $\Pi(\theta)$, the upper bound comes from Eq. (3.19), and θ_0 is assumed to be given for simplicity. Using the bound as a conservative estimate of the prior error, a rule of thumb for informative estimation is

$$\frac{\text{BMSE}_{\mu\mu}}{\theta_0^2 (\Delta/2)^{2|\mu|}} \ll 1. \quad (4.48)$$

The small prior error places a stringent requirement on the measurement. For direct imaging, assuming the asymptotic limit where the BCRB given by Eq. (2.26) is close to the CRB given by Eq. (3.32), the fractional BCRB is

$$\frac{\text{BCRB}_{\mu\mu}}{\text{BMSE}_{\mu\mu}^{(\Pi)}} \approx \frac{\text{CRB}_{\mu\mu}}{\text{BMSE}_{\mu\mu}^{(\Pi)}} = \frac{O(\Delta^{-2|\mu|})}{N}, \quad (4.49)$$

where N is the photon number defined by Eq. (2.16). This value grows exponentially with the order $|\mu|$, meaning that the estimation of higher-order moments requires substantially more photons to become informative.

For SPADE, an achievable Bayesian error can be obtained by averaging $\text{MSE}(\theta'_\mu, \theta_\mu)$, and the magnitude is

also given by Eq. (4.46). The fractional error becomes

$$\frac{\text{BMSE}_{\mu\mu}}{\text{BMSE}_{\mu\mu}^{(\Pi)}} = \frac{O(\Delta^{2[|\mu|/2] - 2|\mu|})}{\min(N_j)} + O(\Delta^4), \quad (4.50)$$

where $N_j \equiv \tau_j \theta_0$ is the average photon number detected by each basis measurement. The $O(\Delta^4)$ relative bias is always low, but the fractional variance still grows with $|\mu|$ exponentially, despite a reduction in the exponent for $|\mu| \geq 2$. While not as many photons are needed to achieve a small fractional error for a given moment, higher-order moments remain more difficult to estimate.

This consideration suggests that SPADE is most useful for scenarios that require only a few low-order moments. For example, the two-point problem studied in Refs. [1–7, 9–18] requires only moments up to the second order [8], the case of two unequal sources studied in Ref. [19] requires moments up to the third, and parametric object models with size and shape parameters [8, 37] can also be related to low-order moments.

V. GAUSSIAN POINT-SPREAD FUNCTION

A. Direct imaging

For an illustrative example of the general theory, consider the Gaussian PSF

$$\psi(x) = \frac{1}{(2\pi)^{d/4}} \exp\left(-\frac{\|x\|^2}{4}\right), \quad (5.1)$$

which is a common assumption in fluorescence microscopy [28, 48]. The orthogonal polynomials with respect to $|\psi(x)|^2$ are well known to be

$$a_\mu(x) = \frac{1}{\sqrt{\mu!}} \text{He}_\mu(x), \quad (5.2)$$

where the multivariate Hermite polynomial is defined as

$$\text{He}_\mu(x) \equiv \prod_{j=1}^D \text{He}_{\mu_j}(x_j), \quad (5.3)$$

and the definition of single-variable Hermite polynomials can be found, for example, in Refs. [49, 50]. To find the b polynomials defined by Eq. (3.8), the generating function for Hermite polynomials [49, 50] can be used to obtain

$$\begin{aligned} |\psi(x - X)|^2 &= \frac{1}{(2\pi)^{d/2}} \exp\left(-\frac{\|x - X\|^2}{2}\right) \\ &= \frac{1}{(2\pi)^{d/2}} \exp\left(-\frac{\|x\|^2}{2}\right) \sum_{\nu} \frac{\text{He}_\nu(x)}{\nu!} X^\nu, \end{aligned} \quad (5.4)$$

which can be substituted into Eq. (3.8), resulting in

$$b_\mu(X) = \frac{1}{\sqrt{\mu!}} X^\mu. \quad (5.6)$$

The β parameters defined by Eq. (3.12) are simply proportional to the moments, viz.,

$$B_{\mu\nu} = \frac{\delta_{\mu\nu}}{\sqrt{\mu!}}, \quad \beta_\mu = \frac{\theta_\mu}{\sqrt{\mu!}}. \quad (5.7)$$

The direct-imaging CRB given by Eq. (3.32) is hence

$$(J^{-1})_{\mu\nu} = \frac{\theta_0}{\tau} [\mu! \delta_{\mu\nu} + O(\Delta)], \quad (5.8)$$

and the near-efficient estimator given by Eq. (3.33) becomes

$$\check{\theta}_\mu = \frac{1}{\tau} \int dm(x) \text{He}_\mu(x), \quad (5.9)$$

which is unbiased and has a variance given by

$$\mathbb{V}_{\mu\nu}(\check{\theta}) = \frac{\theta_0}{\tau} [\mu! \delta_{\mu\nu} + O(\Delta)]. \quad (5.10)$$

These results coincide with the $D = 2$ theory in Ref. [8].

B. Spatial-mode demultiplexing

The PSF in the spatial-frequency domain is given by

$$\Psi(k) = \left(\frac{2}{\pi}\right)^{d/4} \exp(-\|k\|^2). \quad (5.11)$$

The orthogonal polynomials with respect to $|\Psi(k)|^2$ are

$$c_q(k) = \frac{1}{\sqrt{q!}} \text{He}_q(2k). \quad (5.12)$$

Since the Hermite-Gaussian modes are eigenmodes of Fourier transform, the PAD basis in this case is simply the TEM basis, as expected. The propagator given by Eq. (2.7) can again be computed with the help of the Hermite-polynomial generating function; the result is

$$h_q(X) = K_q \exp\left(-\frac{\|X\|^2}{8}\right) X^q, \quad (5.13)$$

$$K_q \equiv \frac{1}{2^{|q|} \sqrt{q!}}. \quad (5.14)$$

This agrees with the general theory that $h_q(X)$ is a polynomial of degree $|q|$ to the leading order. The mutual coherence matrix Γ defined by Eq. (4.8) becomes

$$\Gamma_{qq'} = K_q K_{q'} \int dX \exp\left(-\frac{\|X\|^2}{4}\right) X^{q+q'} F(X|\theta). \quad (5.15)$$

Unbiased estimators of $\Gamma_{qq'}$ can be constructed from projections in the PAD and iPAD spatial modes according to Eqs. (4.10) and (4.17); the iPAD modes are called iTEM modes in Ref. [8]. The estimator variances are given by Eqs. (4.11) and (4.18), with magnitudes given by Eq. (4.28).

Equation (5.15) offers a shortcut to express each moment in terms of Γ as follows:

$$\theta_{q+q'} = \int dX \exp\left(-\frac{\|X\|^2}{4}\right) \exp\left(-\frac{\|X\|^2}{4}\right) X^{q+q'} F(X|\theta) \quad (5.16)$$

$$= \int dX \sum_r \frac{X^{2r}}{r! 4^{|r|}} \exp\left(-\frac{\|X\|^2}{4}\right) X^{q+q'} F(X|\theta) \quad (5.17)$$

$$= \sum_r \frac{1}{r! 4^{|r|}} \int dX \exp\left(-\frac{\|X\|^2}{4}\right) X^{q+q'+2r} F(X|\theta) \quad (5.18)$$

$$= \sum_r \frac{\Gamma_{q+r, q'+r}}{r! 4^{|r|} K_{q+r} K_{q'+r}}. \quad (5.19)$$

The simplified estimator given by Eq. (4.38) becomes

$$\check{\theta}'_{q+q'} = \frac{\check{\Gamma}_{qq'}}{K_q K_{q'}}. \quad (5.20)$$

Given a moment θ_μ , q and $q' = \mu - q$ can be chosen according to Eq. (4.42), and the error then agrees with Eq. (4.46). These results again agree with Ref. [8], except that Ref. [8] neglects the effect of bias on the mean-square error and therefore does not include the second term in Eq. (4.46).

C. Unbiased multi-moment estimation

For $D = 2$, Ref. [8] proposes 7 bases, named TEM and iTEM1–iTEM6, that can be used to estimate all moments via Eq. (5.20). Table I lists their spatial modes and the moment estimators $\{\check{\theta}'_\mu\}$ that they can provide, while Fig. 2 depicts the bases in the mode-index space $q = (q_1, q_2)$.

Interestingly, it is possible to go further than Ref. [8]

Basis	Spatial modes	q_1	q_2	μ_1 of $\check{\theta}'_\mu$	μ_2 of $\check{\theta}'_\mu$
TEM	$\phi_q(x)$	\mathbb{N}_0	\mathbb{N}_0	$2\mathbb{N}_0$	$2\mathbb{N}_0$
iTEM1	$\varphi_{qq'}^\pm(x); q' = q + (1, 0)$	$2\mathbb{N}_0$	\mathbb{N}_0	$4\mathbb{N}_0 + 1$	$2\mathbb{N}_0$
iTEM2	$\varphi_{qq'}^\pm(x); q' = q + (0, 1)$	\mathbb{N}_0	$2\mathbb{N}_0$	$2\mathbb{N}_0$	$4\mathbb{N}_0 + 1$
iTEM3	$\varphi_{qq'}^\pm(x); q' = q + (1, -1)$	\mathbb{N}_0	$2\mathbb{N}_0 + 1$	$2\mathbb{N}_0 + 1$	$4\mathbb{N}_0 + 1$
iTEM4	$\varphi_{qq'}^\pm(x); q' = q + (1, 0)$	$2\mathbb{N}_0 + 1$	\mathbb{N}_0	$4\mathbb{N}_0 + 3$	$2\mathbb{N}_0$
iTEM5	$\varphi_{qq'}^\pm(x); q' = q + (0, 1)$	\mathbb{N}_0	$2\mathbb{N}_0 + 1$	$2\mathbb{N}_0$	$4\mathbb{N}_0 + 3$
iTEM6	$\varphi_{qq'}^\pm(x); q' = q + (1, -1)$	\mathbb{N}_0	$2\mathbb{N}_0$	$2\mathbb{N}_0 + 1$	$4\mathbb{N}_0 + 3$

TABLE I. A list of measurement bases for moment estimation with two-dimensional Gaussian PSF and their spatial modes. Measurement in each basis can provide a set of moment estimators $\{\check{\theta}'_\mu\}$, where the set of $\mu = (\mu_1, \mu_2)$ indices are listed in the last two columns.

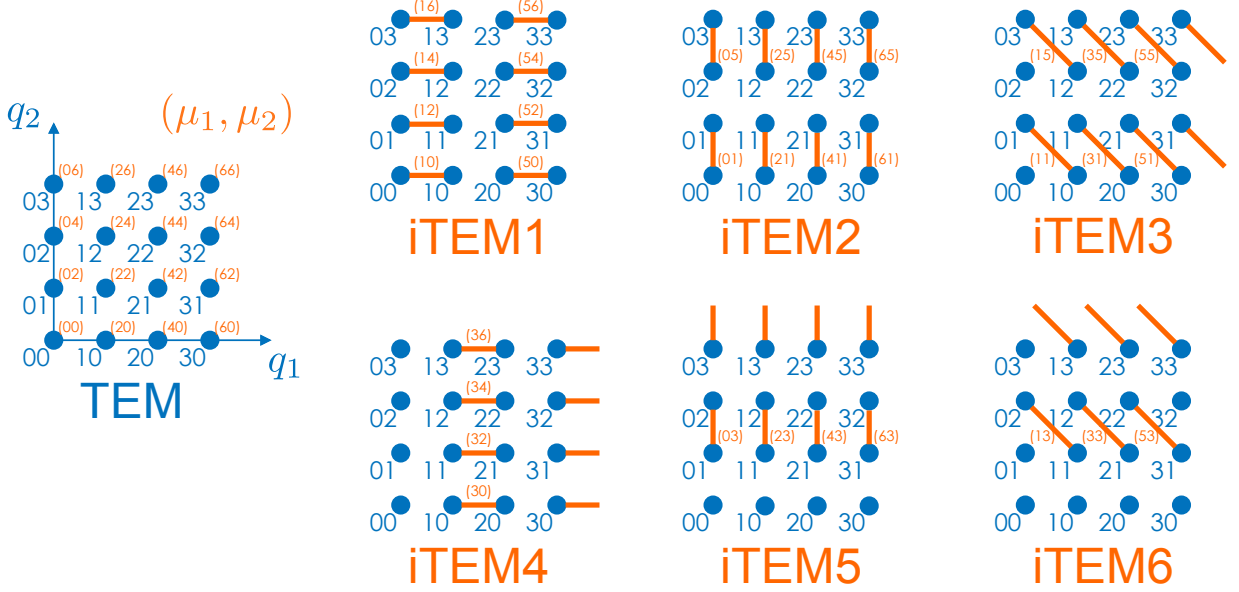


FIG. 2. (Color online). An illustration of the different bases in the TEM and iTEM schemes. Each dot in the (q_1, q_2) space represents a TEM mode, and the TEM modes form a basis in the TEM scheme on the left. In each iTEM scheme, a line connecting two dots represents an interference between the two TEM modes, producing two new modes that replace the original TEM modes in the basis. Each bracketed pair of numbers denote the order (μ_1, μ_2) of the estimator $\check{\theta}'_\mu$ that a projection can provide. The unconnected dots in the iTEM schemes denote TEM modes that should also be measured to provide extra efficiency.

and construct exactly unbiased moment estimators from these measurements. Combining Eqs. (5.19) and (5.20), it can be shown that the estimator

$$\check{\theta}_\mu = \sum_r \frac{\check{\theta}'_{\mu+2r}}{r!4^{|r|}} \quad (5.21)$$

is exactly unbiased. To construct

$$\{\check{\theta}_\mu; \mu \in (2\mathbb{N}_0) \otimes (2\mathbb{N}_0)\}, \quad (5.22)$$

one simply needs $\{\check{\theta}'_\mu; \mu \in (2\mathbb{N}_0) \otimes (2\mathbb{N}_0)\}$ from the TEM scheme. To construct

$$\{\check{\theta}_\mu; \mu \in (2\mathbb{N}_0 + 1) \otimes (2\mathbb{N}_0)\}, \quad (5.23)$$

one needs $\{\check{\theta}'_\mu; \mu \in (2\mathbb{N}_0 + 1) \otimes (2\mathbb{N}_0)\}$, which can be obtained from the iTEM1 and iTEM4 schemes. Similarly,

to construct

$$\{\check{\theta}_\mu; \mu \in (2\mathbb{N}_0) \otimes (2\mathbb{N}_0 + 1)\}, \quad (5.24)$$

one needs $\{\check{\theta}'_\mu; \mu \in (2\mathbb{N}_0) \otimes (2\mathbb{N}_0 + 1)\}$, which can be obtained from the iTEM2 and iTEM5 schemes. Finally, to construct

$$\{\check{\theta}_\mu; \mu \in (2\mathbb{N}_0 + 1) \otimes (2\mathbb{N}_0 + 1)\}, \quad (5.25)$$

one needs $\{\check{\theta}'_\mu; \mu \in (2\mathbb{N}_0 + 1) \otimes (2\mathbb{N}_0 + 1)\}$, which can be obtained from the iTEM3 and iTEM6 schemes. The error covariance matrix of the unbiased estimator becomes

$$\text{MSE}_{\mu\nu}(\check{\theta}, \theta) = \mathbb{V}_{\mu\nu}(\check{\theta}) = \frac{\theta_0}{\min(\tau_j)} O(\Delta^{2[|\mu|/2]}) \delta_{\mu\nu}, \quad (5.26)$$

which remains much lower than the direct-imaging CRB given by Eq. (3.32) for $\Delta \ll 1$ and $|\mu| \geq 2$, while the bias contribution in Eq. (4.46) is no longer present.

Since the 7 bases are incompatible, each scheme has its own conversion factor τ_j , and energy conservation mandates that

$$\min(\tau_j) \leq \frac{T}{7\hbar\omega_0}, \quad (5.27)$$

if all 7 measurement schemes are performed. Still, the dependence of the errors on $O(\Delta^{2\lfloor|\mu|/2\rfloor})$ implies that substantial enhancements remain possible in the subdiffraction regime. For other PSFs and other dimensions, the number of bases needed to achieve enhanced and exactly unbiased multi-moment estimation remains an open question.

VI. NUMERICAL DEMONSTRATION

I now present Monte Carlo simulations to corroborate the theory. Assume $D = 1$. The simulated object is a collection of $S = 5$ point sources with randomly generated positions within the interval

$$|X_s| \leq \frac{\Delta}{2}, \quad \Delta = 0.2, \quad (6.1)$$

such that

$$F(X|\theta) = \frac{\theta_0}{S} \sum_{s=1}^S \delta(X - X_s). \quad (6.2)$$

The average photon number is $N = \tau\theta_0 = 50,000$. For direct imaging, the pixel size is $dx = 0.1$, and 1,000 samples of Poisson images are generated for each object. The unbiased estimator given by Eq. (3.33) is applied to each sample to estimate the moments up to $\mu = 4$. The mean-square errors with respect to the true parameters are averaged to approximate the expected values. The averaged errors are then plotted in Figs. 3–4 for two different PSFs and compared with the CRBs

$$\text{CRB}_{\mu\mu} \approx \frac{\theta_0}{\tau} \sum_{\xi} [(B^{-1})_{\mu\xi}]^2, \quad (6.3)$$

omitting the $O(\Delta)$ correction in Eq. (3.32).

For SPADE described in Sec. IV A, measurements in three different bases are simulated. The first basis is

$$\{\phi_0(x), \phi_1(x), \phi_2(x)\}, \quad (6.4)$$

which produces photon counts $\{m_0, m_1, m_2\}$, the second basis is

$$\{\varphi_{01}^+(x), \varphi_{01}^-(x), \phi_2(x)\}, \quad (6.5)$$

with photon counts $\{m_{01}^+, m_{01}^-, m_2'\}$, and the third basis is

$$\{\phi_0(x), \varphi_{12}^+(x), \varphi_{12}^-(x)\}, \quad (6.6)$$

with photon counts $\{m_0', m_{12}^+, m_{12}^-\}$. The light is split equally among the three measurements, such that

$$\tau_j = \frac{\tau}{3}, \quad N_j = \tau_j \theta_0 = \frac{N}{3}. \quad (6.7)$$

All photons in higher-order modes are neglected. To estimate θ_0 , I simply sum all the photon counts. The resulting error is almost identical to that obtained by direct imaging. This is expected, as SPADE loses very few photons to the neglected higher-order modes and its total efficiency is taken to be almost identical to that of direct imaging. To estimate θ_1 , I use the simplified but biased estimator given by Eq. (4.38), with q given by Eq. (4.42). For $D = 1$, it can be further simplified to give

$$\check{\theta}'_1 = \frac{m_{01}^+ - m_{01}^-}{2H_{00}H_{11}\tau_j}. \quad (6.8)$$

The simulated errors are computed with respect to the true parameters, averaged over 1,000 samples, and compared with the analytic expression

$$\text{MSE}_{11} \approx \mathbb{V}(\check{\theta}'_1) \approx \frac{\Gamma_{00}}{4H_{00}^2H_{11}^2\tau_j} \approx \frac{\theta_0}{4H_{11}^2\tau_j}, \quad (6.9)$$

which neglects the bias. Similarly, to estimate θ_2 and θ_3 , I assume

$$\check{\theta}'_2 = \frac{m_1}{H_{11}^2\tau_j}, \quad \text{MSE}_{22} \approx \frac{\theta_2}{H_{11}^2\tau_j}. \quad (6.10)$$

$$\check{\theta}'_3 = \frac{m_{12}^+ - m_{12}^-}{2H_{11}H_{22}\tau_j}, \quad \text{MSE}_{33} \approx \frac{\theta_2}{4H_{22}^2\tau_j}. \quad (6.11)$$

To estimate θ_4 , I use both of the photon counts that come from the two $\phi_2(x)$ projections, viz.,

$$\check{\theta}'_4 = \frac{m_2 + m_2'}{2H_{22}^2\tau_j}, \quad \text{MSE}_{44} \approx \frac{\theta_4}{2H_{22}^2\tau_j}. \quad (6.12)$$

The simulated errors and the analytic expressions are plotted in Figs. 3–5 against the relevant parameters in log-log scale for three different PSFs.

Figure 3 plots the results for the Gaussian PSF described in Sec. V. The results for $\mu = 0$ are trivial and not shown. The simulated errors all match the theory, despite the approximations in the analytic expressions. In particular, they confirm that the contribution of bias to the errors of SPADE is indeed negligible. For $\mu = 1$, SPADE uses one third of the photons only, so its errors are three times those of direct imaging. For higher moments, however, SPADE outperforms direct imaging by orders of magnitude.

It is important to note that the plotted errors are normalized with respect to the prior $\theta_0^2(\Delta/2)^{2\mu}$, and only the normalized errors for $\mu = 1, 2$ (and $\mu = 0$) go significantly below 1. According to the discussion in Sec. IV C, this implies that only the estimation for $\mu \leq 2$ is informative, while the estimation for $\mu \geq 3$ would require a lot more photons to become informative. The high variances of

the estimators for $\mu \geq 3$ also suggest that, for the given photon number, replacing them with Bayesian estimators [22, 45, 47] can reduce their errors to the vicinity of the prior levels given by Eq. (4.47), at the expense of unbiasedness.

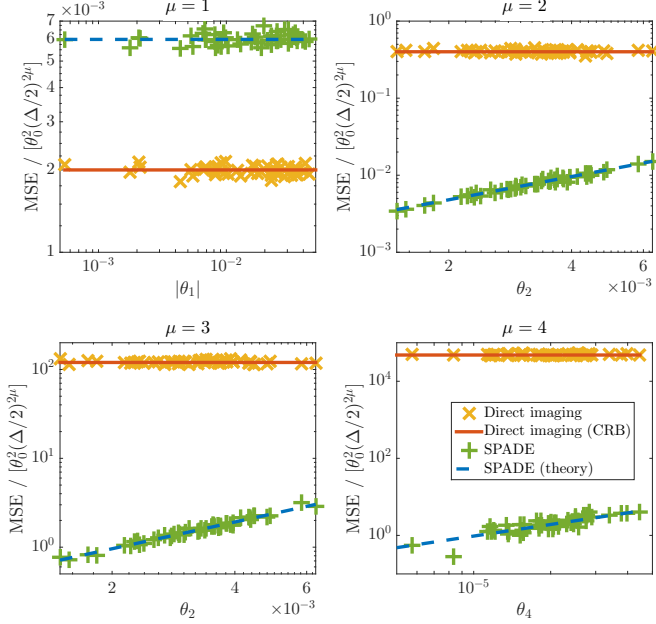


FIG. 3. (Color online). Simulated and theoretical errors of moment estimation via direct imaging and SPADE for the Gaussian PSF. The discrete points are from the Monte Carlo simulations and the lines are from the analytic theory. All axes are normalized, dimensionless, and in logarithmic scale. See the main text for details.

For another example, consider the “bump” aperture function

$$\Psi(k) = \begin{cases} \Psi(0) \exp\left(-\frac{k^2}{1-k^2}\right), & |k| < 1, \\ 0, & |k| \geq 1, \end{cases} \quad (6.13)$$

where $\Psi(0) \approx 1.0084$ is a normalization constant. The differentiability of $\Psi(k)$ ensures that the relevant moments of $|\psi(x)|^2$ used to define the a polynomials are finite, at least up to $\mu = 4$. The results, plotted in Fig. 4, behave similarly to those in the Gaussian case, except that the direct-imaging errors are substantially higher for higher moments. The enhancements by SPADE appear even bigger, though not big enough to bring the errors for $\mu \geq 3$ down to the informative regime for the given photon number.

For the final example, consider the textbook rectangle aperture function

$$\Psi(k) = \begin{cases} 1, & |k| < 1/2, \\ 0, & |k| \geq 1/2. \end{cases} \quad (6.14)$$

The second and higher moments of $|\psi(x)|^2$ are infinite, meaning the a polynomials are undefined and the direct-imaging CRBs derived in Sec. III are inapplicable. Fortunately, the orthogonal polynomials with respect to

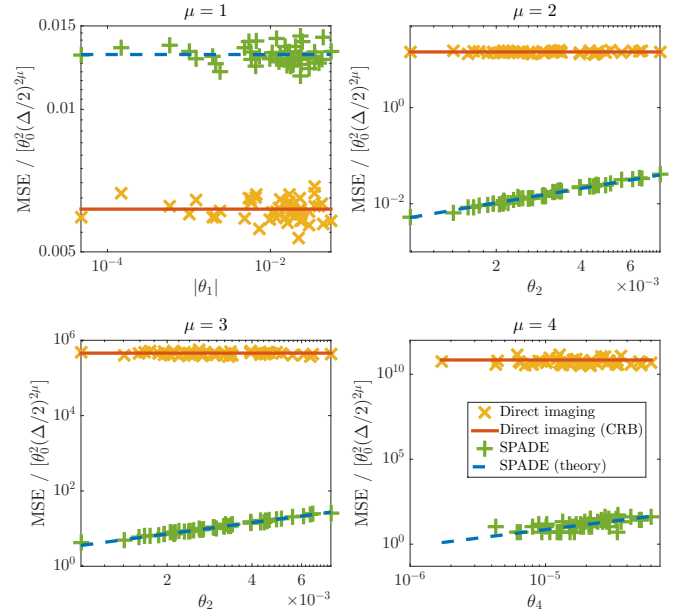


FIG. 4. (Color online). Simulated and theoretical errors of moment estimation via direct imaging and SPADE for the bump aperture given by Eq. (6.13). The format of the plots is identical to that of Fig. 3. See the main text for details.

$|\Psi(k)|^2$ and therefore the PAD basis remain well-defined [15]. Figure 5 plots the results for SPADE, which are similar to those for the bump aperture in Fig. 4. Although these results have no direct-imaging limits to compare with, the earlier results on the two-point problem for this PSF [1, 14, 15] suggest that significant improvements remain likely.

VII. CONCLUSION

The semiclassical treatment complements the quantum approach in Ref. [8] by offering a shortcut to the Poisson photon-counting model for incoherent sources, passive linear optics, and photon counting. Besides pedagogy, this work generalizes the results in Refs. [1–19] for more general objects and PSFs in the context of moment estimation, demonstrating that the giant enhancement by SPADE is not limited to the case of two point sources or Gaussian PSF considered in prior works.

Many open problems remain, such as the effect of excess errors, the imaging of more complex objects, the application of more advanced Bayesian or minimax statistics [22, 24, 33–40, 45], and the quantum optimality of the measurements [51, 52]. Experimental implementation is another important future direction. For proof-of-concept demonstrations, it should be possible to use the same setups described in Refs. [11–14] to estimate at least the second moments of more general objects. For practical applications in astronomy and fluorescence microscopy, efficient demultiplexing for broadband sources is needed.

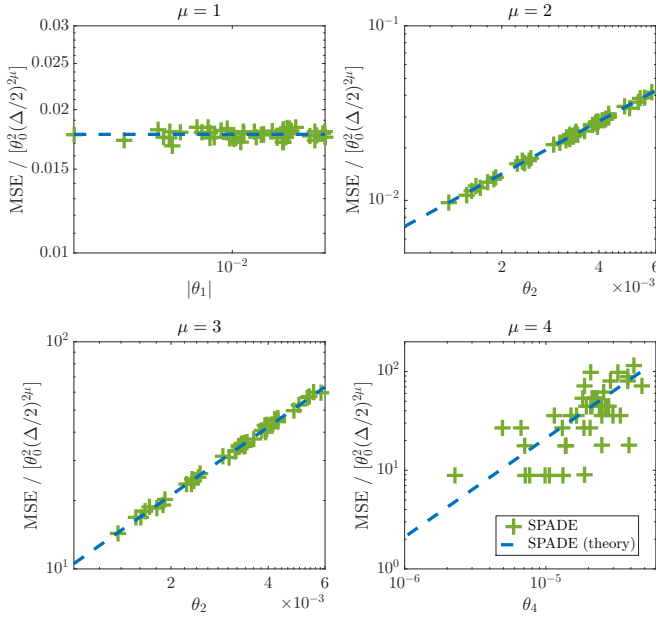


FIG. 5. (Color online). Simulated and theoretical errors of moment estimation via SPADE for the rectangle aperture given by Eq. (6.14). The format of the plots is identical to that of Figs. 3 and 4. Note that the spread of errors for $\mu = 4$ looks more severe because the range of the vertical axis is smaller than those of the other $\mu = 4$ plots in Figs. 3 and 4. Also, relatively few photons from a subdiffraction object are coupled into the $\phi_2(x)$ mode, so the error itself has a high variance and more samples would be required for the average errors to get closer to the expected values.

The technical challenge is by no means trivial, but the experimental progress on spatial-mode demultiplexers has been encouraging [11, 14, 53–59], and the promise of giant enhancements using only far-field linear optics should motivate further efforts.

ACKNOWLEDGMENTS

This work is supported by the Singapore Ministry of Education Academic Research Fund Tier 1 Project R-263-000-C06-112.

Appendix A: Multi-index notation

A D -dimensional vector of continuous variables is written as

$$x = (x_1, x_2, \dots, x_D) \in \mathbb{R}^D. \quad (\text{A1})$$

For such a vector, the following notations are assumed:

$$\begin{aligned} dx &\equiv \prod_{j=1}^D dx_j, & \int dx &\equiv \int_{\mathbb{R}^D} dx, \\ \delta(x - x') &\equiv \prod_{j=1}^D \delta(x_j - x'_j), & \partial_x &\equiv \left(\frac{\partial}{\partial x_1}, \dots, \frac{\partial}{\partial x_D} \right), \\ k \cdot x &\equiv \sum_{j=1}^D k_j x_j, & ||x|| &\equiv \sqrt{x \cdot x}. \end{aligned} \quad (\text{A2})$$

If the subscript is omitted in ∂ , derivatives with respect to x are assumed.

A vector of integer indices, on the other hand, is defined as

$$\mu = (\mu_1, \mu_2, \dots, \mu_D) \in \mathbb{N}_0^D. \quad (\text{A3})$$

For such a vector, the following notations are assumed:

$$\begin{aligned} 0 &\equiv (0, \dots, 0), & \sum_{\mu=\nu}^{\xi} &\equiv \sum_{\mu=\nu_1}^{\xi_1} \dots \sum_{\mu=\nu_D}^{\xi_D}, \\ \sum_{\mu} &\equiv \sum_{\mu \in \mathbb{N}_0^D}, & |\mu| &\equiv \sum_{j=1}^D |\mu_j|, \\ \mu! &\equiv \prod_{j=1}^D \mu_j!, & \binom{\mu}{\nu} &\equiv \frac{\mu!}{(\mu - \nu)! \nu!}. \end{aligned} \quad (\text{A4})$$

Other useful notations include

$$x^{\mu} \equiv \prod_{j=1}^D x_j^{\mu_j}, \quad \partial_x^{\mu} \equiv \prod_{j=1}^D \frac{\partial^{\mu_j}}{\partial x_j^{\mu_j}}. \quad (\text{A5})$$

Appendix B: Properties of some matrices in the main text

The lower-triangular A matrix specifies the orthogonal polynomials a defined by Eqs. (3.3) and (3.6), which can be combined to give

$$\sum_{\xi, \zeta} A_{\mu\xi} M_{\xi\zeta} A_{\nu\zeta} = \delta_{\mu\nu}, \quad (\text{B1})$$

where

$$M_{\xi\zeta} = \lambda_{\xi+\zeta} \equiv \int dx |\psi(x)|^2 x^{\xi+\zeta} \quad (\text{B2})$$

is the moment matrix. For orthogonal polynomials to exist, M should be positive-definite [23], or equivalently

$$\int dx |\psi(x)|^2 \mathcal{P}^2(x) > 0 \quad (\text{B3})$$

for any polynomial \mathcal{P} . The strict positiveness can be satisfied as long as $|\psi(x)|^2$ is not a discrete measure, as

$\mathcal{P}^2(x)$ goes to zero at discrete points only. Equation (B1) then implies that A can be obtained from the Cholesky decomposition

$$M = LL^\top, \quad (\text{B4})$$

where \top denotes the transpose and L is a real lower-triangular matrix with positive diagonal entries [60]. Since the diagonal entries of a triangular matrix are also its eigenvalues, L is invertible, L^{-1} is also a lower-triangular matrix, and setting

$$A = L^{-1} \quad (\text{B5})$$

satisfies Eq. (B1). The diagonal entries are related by

$$A_{\mu\mu} = \frac{1}{L_{\mu\mu}} > 0. \quad (\text{B6})$$

B specifies the b polynomial and given by Eq. (3.10). Its lower-triangular property can be proved by observing that Eq. (3.10) depends on

$$\partial^\nu a_\mu(x) = \sum_\xi A_{\mu\xi} \partial^\nu x^\xi, \quad (\text{B7})$$

where $A_{\mu\xi} = 0$ for $\xi > \mu$, and $\nu > \mu \geq \xi$ in the graded lexicographical order implies that at least one $\nu_j > \mu_j \geq \xi_j$, causing Eq. (B7) to vanish. The diagonal entries of B are

$$B_{\mu\mu} = \int dx |\psi(x)|^2 A_{\mu\mu} = A_{\mu\mu}. \quad (\text{B8})$$

Since $A_{\mu\mu} > 0$,

$$\det B = \prod_\mu B_{\mu\mu} = \prod_\mu A_{\mu\mu} > 0, \quad (\text{B9})$$

B is invertible, and B^{-1} is also lower-triangular. Another way of writing B is

$$B_{\mu\nu} = \sum_\xi A_{\mu\xi} \begin{pmatrix} \xi \\ \nu \end{pmatrix} \lambda_{\xi-\nu} \quad (\text{B10})$$

in terms of the moments, which is useful for its computation.

The lower-triangular C matrix specifies the orthogonal polynomials c defined by Eqs. (4.5) and (4.6), which can be combined to give

$$\sum_{s,t} C_{qs} \Lambda_{st} C_{rt} = \delta_{qr}, \quad (\text{B11})$$

where

$$\Lambda_{st} \equiv \int dk |\Psi(k)|^2 k^{s+t} \quad (\text{B12})$$

is another moment matrix. Assume that Λ is positive-definite. Similar to A , C can be obtained by Cholesky decomposition, and both C and C^{-1} are lower-triangular with positive diagonal entries.

Consider now the H matrix defined in Eq. (4.22). Inverting Eq. (4.5) to obtain

$$k^r = \sum_s (C^{-1})_{rs} c_s(k), \quad (\text{B13})$$

substituting this in Eq. (4.22), and using the orthonormality given by Eq. (4.6), I obtain

$$H_{qr} = \frac{i^{|q|}(-i)^{|r|}}{r!} \sum_s (C^{-1})_{rs} \int dk |\Psi(k)|^2 c_q(k) c_s(k) \quad (\text{B14})$$

$$= \frac{i^{|q|}(-i)^{|r|}}{r!} (C^{-1})_{rq}. \quad (\text{B15})$$

The inverse is given by Eq. (4.24), which can be confirmed by directly computing HH^{-1} . Since C^{-1} and C are lower-triangular, H and H^{-1} are upper-triangular.

If $|\Psi(k)|^2$ is centrally symmetric according to Eq. (4.16), Ref. [23] shows that $c_q(k)$ consists of only even-order monomials $\{k^r; |r| \text{ even}\}$ if $|q|$ is even and only odd-order monomials $\{k^r; |r| \text{ odd}\}$ if $|q|$ is odd. Thus

$$C_{qr} = 0 \text{ if } |q| - |r| \text{ is odd}, \quad (\text{B16})$$

$$c_q(k) = (-1)^{|q|} c_q(-k). \quad (\text{B17})$$

Substituting $k \rightarrow -k$ for the integral in Eq. (4.19) yields

$$h_q(X) = i^{|q|} \int dk |\Psi(k)|^2 c_q(k) \exp(-ik \cdot X) \quad (\text{B18})$$

$$= i^{|q|} \int dk |\Psi(-k)|^2 c_q(-k) \exp(ik \cdot X) \quad (\text{B19})$$

$$= (-i)^{|q|} \int dk |\Psi(k)|^2 c_q(k) \exp(ik \cdot X) \quad (\text{B20})$$

$$= h_q^*(X), \quad (\text{B21})$$

and $h_q(X)$ is real. It follows that H and H^{-1} are real as well.

[1] Mankei Tsang, Ranjith Nair, and Xiao-Ming Lu, “Quantum theory of superresolution for two incoherent optical

point sources,” *Physical Review X* **6**, 031033 (2016).

[2] Ranjith Nair and Mankei Tsang, “Interferometric super-

- localization of two incoherent optical point sources,” *Optics Express* **24**, 3684–3701 (2016).
- [3] Mankei Tsang, Ranjith Nair, and Xiao-Ming Lu, “Quantum information for semiclassical optics,” in *Proc. SPIE*, Quantum and Nonlinear Optics IV, Vol. 10029 (SPIE, Bellingham, WA, 2016) p. 1002903.
 - [4] Ranjith Nair and Mankei Tsang, “Far-Field Superresolution of Thermal Electromagnetic Sources at the Quantum Limit,” *Physical Review Letters* **117**, 190801 (2016).
 - [5] Cosmo Lupo and Stefano Pirandola, “Ultimate Precision Bound of Quantum and Subwavelength Imaging,” *Physical Review Letters* **117**, 190802 (2016).
 - [6] Mankei Tsang, “Conservative classical and quantum resolution limits for incoherent imaging,” *Journal of Modern Optics* **65**, 104–110 (2018).
 - [7] Shan Zheng Ang, Ranjith Nair, and Mankei Tsang, “Quantum limit for two-dimensional resolution of two incoherent optical point sources,” *Physical Review A* **95**, 063847 (2017).
 - [8] Mankei Tsang, “Subdiffraction incoherent optical imaging via spatial-mode demultiplexing,” *New Journal of Physics* **19**, 023054 (2017).
 - [9] Hari Krovi, Saikat Guha, and Jeffrey H. Shapiro, “Attaining the quantum limit of passive imaging,” [arXiv:1609.00684 \[physics, physics:quant-ph\]](https://arxiv.org/abs/1609.00684) (2016).
 - [10] Xiao-Ming Lu, Ranjith Nair, and Mankei Tsang, “Quantum-optimal detection of one-versus-two incoherent sources with arbitrary separation,” [arXiv:1609.03025 \[quant-ph\]](https://arxiv.org/abs/1609.03025) (2016).
 - [11] Weng-Kian Tham, Hugo Ferretti, and Aephraim M. Steinberg, “Beating Rayleigh’s Curse by Imaging Using Phase Information,” *Physical Review Letters* **118**, 070801 (2017).
 - [12] Zong Sheng Tang, Kadir Durak, and Alexander Ling, “Fault-tolerant and finite-error localization for point emitters within the diffraction limit,” *Optics Express* **24**, 22004 (2016).
 - [13] Fan Yang, Arina Tashchilina, E. S. Moiseev, Christoph Simon, and A. I. Lvovsky, “Far-field linear optical superresolution via heterodyne detection in a higher-order local oscillator mode,” *Optica* **3**, 1148 (2016).
 - [14] Martin Paúr, Bohumil Stoklasa, Zdenek Hradil, Luis L. Sánchez-Soto, and Jaroslav Rehacek, “Achieving the ultimate optical resolution,” *Optica* **3**, 1144 (2016).
 - [15] J. Rehacek, M. Paúr, B. Stoklasa, Z. Hradil, and L. L. Sánchez-Soto, “Optimal measurements for resolution beyond the Rayleigh limit,” *Optics Letters* **42**, 231–234 (2017).
 - [16] Fan Yang, Ranjith Nair, Mankei Tsang, Christoph Simon, and Alexander I. Lvovsky, “Fisher information for far-field linear optical superresolution via homodyne or heterodyne detection in a higher-order local oscillator mode,” [arXiv:1706.08633 \[physics, physics:quant-ph\]](https://arxiv.org/abs/1706.08633) (2017).
 - [17] Ronan Kerviche, Saikat Guha, and Amit Ashok, “Fundamental limit of resolving two point sources limited by an arbitrary point spread function,” [arXiv:1701.04913 \[physics, physics:quant-ph\]](https://arxiv.org/abs/1701.04913) (2017).
 - [18] Andrzej Chrostowski, Rafał Demkowicz-Dobrzański, Marcin Jarzyna, and Konrad Banaszek, “On super-resolution imaging as a multiparameter estimation problem,” *International Journal of Quantum Information*, 1740005 (2017).
 - [19] J. Rehacek, Z. Hradil, B. Stoklasa, M. Paúr, J. Grover, A. Krzic, and L. L. Sanchez-Soto, “Multiparameter Quantum Metrology of Incoherent Point Sources: Towards Realistic Superresolution,” [arXiv:1709.07705 \[quant-ph\]](https://arxiv.org/abs/1709.07705) (2017).
 - [20] Joseph W. Goodman, *Introduction to Fourier Optics* (McGraw-Hill, New York, 2004).
 - [21] Joseph W. Goodman, *Statistical Optics* (Wiley, New York, 1985).
 - [22] Harry L. Van Trees, *Detection, Estimation, and Modulation Theory, Part I* (John Wiley & Sons, New York, 2001).
 - [23] Charles F. Dunkl and Yuan Xu, *Orthogonal Polynomials of Several Variables* (Cambridge University Press, Cambridge, 2001).
 - [24] D. R. Cox and D. V. Hinkley, *Theoretical Statistics* (Chapman & Hall/CRC, Boca Raton, 1979).
 - [25] Jonas Zmuidzinas, “Cramér–Rao sensitivity limits for astronomical instruments: implications for interferometer design,” *Journal of the Optical Society of America A* **20**, 218–233 (2003).
 - [26] Martin C. E. Huber, Anuschka Pauluhn, J. Len Culhane, J. Gethyn Timothy, Klaus Wilhelm, and Alex Zehnder, eds., *Observing Photons in Space: A Guide to Experimental Space Astronomy* (Springer, New York, 2013).
 - [27] Eric D. Feigelson and G. Jogesh Babu, *Modern Statistical Methods for Astronomy* (Cambridge University Press, Cambridge, 2012).
 - [28] Jerry Chao, E. Sally Ward, and Raimund J. Ober, “Fisher information theory for parameter estimation in single molecule microscopy: tutorial,” *Journal of the Optical Society of America A* **33**, B36 (2016).
 - [29] Alex von Diezmann, Yoav Shechtman, and W. E. Moerner, “Three-Dimensional Localization of Single Molecules for Super-Resolution Imaging and Single-Particle Tracking,” *Chemical Reviews* **117**, 7244–7275 (2017).
 - [30] David J. Brady, *Optical Imaging and Spectroscopy* (Wiley, Hoboken, 2009).
 - [31] Geoffrey de Villiers and E. Roy Pike, *The Limits of Resolution* (CRC Press, Boca Raton, 2016).
 - [32] James B. Pawley, ed., *Handbook of Biological Confocal Microscopy* (Springer, New York, 2006).
 - [33] M. Raginsky, R. M. Willett, Z. T. Harmany, and R. F. Marcia, “Compressed Sensing Performance Bounds Under Poisson Noise,” *IEEE Transactions on Signal Processing* **58**, 3990–4002 (2010).
 - [34] Johann de Castro and Fabrice Gamboa, “Exact reconstruction using Beurling minimal extrapolation,” *Journal of Mathematical Analysis and Applications* **395**, 336–354 (2012).
 - [35] Emmanuel J. Candès and Carlos Fernandez-Granda, “Towards a Mathematical Theory of Super-resolution,” *Communications on Pure and Applied Mathematics* **67**, 906–956 (2014).
 - [36] Geoffrey Schiebinger, Elina Robeva, and Benjamin Recht, “Superresolution without separation,” *Information and Inference: A Journal of the IMA*, iax006 (2017).
 - [37] Matthew Bierbaum, Brian D. Leahy, Alexander A. Alemi, Itai Cohen, and James P. Sethna, “Light Microscopy at Maximal Precision,” *Physical Review X* **7**, 041007 (2017).
 - [38] Raymond J. Carroll and Peter Hall, “Optimal Rates of Convergence for Deconvolving a Density,” *Journal of the American Statistical Association* **83**, 1184–1186 (1988).

- [39] Jianqing Fan, “On the Optimal Rates of Convergence for Nonparametric Deconvolution Problems,” *The Annals of Statistics* **19**, 1257–1272 (1991).
- [40] Peter Hall and Soumendra N. Lahiri, “Estimation of Distributions, Moments and Quantiles in Deconvolution Problems,” *The Annals of Statistics* **36**, 2110–2134 (2008).
- [41] David A. B. Miller, “All linear optical devices are mode converters,” *Optics Express* **20**, 23985–23993 (2012).
- [42] S. Van Aert, A. J. den Dekker, D. Van Dyck, and A. van den Bos, “High-resolution electron microscopy and electron tomography: resolution versus precision,” *Journal of Structural Biology* **138**, 21–33 (2002).
- [43] M. P. Schützenberger, “A generalization of the Fréchet-Cramér inequality to the case of Bayes estimation,” *Bull. Amer. Math. Soc.* **63**, 142 (1957).
- [44] Richard D. Gill and Boris Y. Levit, “Applications of the Van Trees inequality: A Bayesian Cramér-Rao bound,” *Bernoulli* **1**, 59–79 (1995).
- [45] Harry L. Van Trees and Kristine L. Bell, eds., *Bayesian Bounds for Parameter Estimation and Nonlinear Filtering/Tracking* (Wiley-IEEE, Piscataway, 2007).
- [46] Ram Zamir, “A proof of the Fisher information inequality via a data processing argument,” *IEEE Transactions on Information Theory* **44**, 1246–1250 (1998).
- [47] James O. Berger, *Statistical Decision Theory and Bayesian Analysis* (Springer-Verlag, New York, 1985).
- [48] Bo Zhang, Josiane Zerubia, and Jean-Christophe Olivo-Marin, “Gaussian approximations of fluorescence microscope point-spread function models,” *Applied Optics* **46**, 1819–1829 (2007).
- [49] DLMF, “NIST Digital Library of Mathematical Functions,” <http://dlmf.nist.gov/>, Release 1.0.11 of 2016-06-08 (2016), online companion to [50].
- [50] Frank W. J. Olver, Daniel W. Lozier, Ronald F. Boisvert, and Charles W. Clark, eds., *NIST Handbook of Mathematical Functions* (Cambridge University Press, New York, NY, 2010) print companion to [49].
- [51] Carl W. Helstrom, *Quantum Detection and Estimation Theory* (Academic Press, New York, 1976).
- [52] Alexander S. Holevo, *Probabilistic and Statistical Aspects of Quantum Theory* (Edizioni della Normale, Pisa, Italy, 2011).
- [53] Jean-François Morizur, Lachlan Nicholls, Pu Jian, Seiji Armstrong, Nicolas Treps, Boris Hage, Magnus Hsu, Warwick Bowen, Jiri Janousek, and Hans-A. Bachor, “Programmable unitary spatial mode manipulation,” *J. Opt. Soc. Am. A* **27**, 2524–2531 (2010).
- [54] Guifang Li, Neng Bai, Ningbo Zhao, and Cen Xia, “Space-division multiplexing: the next frontier in optical communication,” *Advances in Optics and Photonics* **6**, 413–487 (2014).
- [55] Lian-Wee Luo, Noam Ophir, Christine P. Chen, Lucas H. Gabrielli, Carl B. Poitras, Keren Bergmen, and Michal Lipson, “WDM-compatible mode-division multiplexing on a silicon chip,” *Nature Communications* **5**, 3069 (2014).
- [56] Aseema Mohanty, Mian Zhang, Avik Dutt, Sven Ramelow, Paulo Nussenzveig, and Michal Lipson, “Quantum interference between transverse spatial waveguide modes,” *Nature Communications* **8**, 14010 (2017).
- [57] Lane Martin, Davood Mardani, H. Esat Kondakci, Walker D. Larson, Soroush Shabahang, Ali K. Jahromi, Tanya Malhotra, A. Nick Vamivakas, George K. Atia, and Ayman F. Abouraddy, “Basis-neutral Hilbert-space analyzers,” *Scientific Reports* **7**, 44995 (2017).
- [58] Mohammad Mirhosseini, Mehul Malik, Zhimin Shi, and Robert W. Boyd, “Efficient separation of the orbital angular momentum eigenstates of light,” *Nature Communications* **4**, 2781 (2013).
- [59] Yiyu Zhou, Mohammad Mirhosseini, Dongzhi Fu, Jiapeng Zhao, Seyed Mohammad Hashemi Rafsanjani, Alan E. Willner, and Robert W. Boyd, “Sorting photons by radial quantum number,” [arXiv:1711.08120 \[physics, physics:quant-ph\]](https://arxiv.org/abs/1711.08120) (2017).
- [60] Roger A. Horn and Charles R. Johnson, *Matrix Analysis* (Cambridge University Press, Cambridge, 1985).